



## Comparative study of mesoporous silica obtained by different synthetic routes to improve the analysis of Cu(II) in sugar cane spirit

Estudo comparativo de sílicas mesoporosas obtidas através de diferentes rotas de síntese para a melhora na análise de Cu(II) em cachaça

J. B. S. Lima<sup>1,2</sup>; S. W. M. M. de Carvalho<sup>1,2</sup>; P. C. A. Santana<sup>1,2</sup>; J. O. S. Silva<sup>1,2</sup>; E. Santos<sup>1</sup>; D. O. Santos<sup>2,3</sup>; M. R. Alexandre<sup>1</sup>; E. M. Sussuchi<sup>1,2\*</sup>

<sup>1</sup> Postgraduate Program in Chemistry, Department of Chemistry, Federal University of Sergipe, 49100-000, São Cristóvão-SE, Brazil.

<sup>2</sup> Corrosion and Nanotechnology Laboratory -LCNT/NUPEG, Federal University of Sergipe, 49100-000, São Cristóvão-SE, Brazil.

<sup>3</sup> Postgraduate Program in Materials Science and Engineering, Federal University of Sergipe, 49100-000, São Cristóvão-SE, Brazil.

\*esmidori@gmail.com

(Recebido em 06 de novembro de 2019; aceito em 01 de março de 2020)

Mesoporous silicas have properties that allow their wide chemical application, due to the large amount of silanol groups on their walls. The possibility of introducing functional groups inside and on the surface of their pores becomes viable the use of these functionalized mesoporous materials for the adsorption of metal ions. Copper ions are essential for vital functions, but in high concentrations, they are responsible for causing problems to the human organism. Therefore, it is important to monitor the species in different media, such as sugar cane spirit. Mesoporous materials type MCM-41 functionalized were obtained by three different methods using direct (in situ) and indirect (post-synthesis) routes. The mesoporous materials have exhibited properties according to the IUPAC classification. Modified carbon paste electrodes (MCPEs) were prepared by immobilizing the synthesized materials for Cu<sup>2+</sup> analysis. The modified electrode obtained by the immobilization of functionalized mesoporous R2 (MCPE/R2) presented the best sensitivity for Cu<sup>2+</sup> detection. Under optimum experimental conditions, the MCPE/R2 exhibited a linear range in between 0.99 and 11.80 μmol L<sup>-1</sup>, a sensitivity based on the Limit of Detection (LOD) of 0.50 μmol L<sup>-1</sup> and Limit of Quantification (LOQ) of 0.99 μmol L<sup>-1</sup>, precision (DPR<sub>máx</sub>) equals to 10.6% and recovery of 92.2%. The developed method proved to be efficient for Cu<sup>2+</sup> determination in sugar cane spirit and the accuracy of the results were comparable to those obtained by AAS.

Keywords: Electrochemistry detection, copper, sugar cane spirit.

Sílicas mesoporosas possuem propriedades que permitem a sua vasta aplicação química, devido a grande quantidade de grupos silanóis em suas paredes. A possibilidade de introdução de grupos funcionais no interior e na superfície dos seus poros, torna-se viável o uso desses materiais mesoporosos funcionalizados para a adsorção de íons metálicos. Os íons Cu<sup>2+</sup> são essenciais para funções vitais, mas em altas concentrações, são responsáveis por causar problemas ao organismo humano. Portanto, é importante o monitoramento da espécie em diversos meios como, em cachaças de cana de açúcar. Materiais mesoporosos funcionalizados do tipo MCM-41 foram obtidos através de três métodos diferentes utilizando rotas diretas (*in situ*) e indiretas (pós-síntese). Os materiais mesoporosos apresentaram propriedades de acordo com a classificação da IUPAC. Eletrodos de pasta de carbono modificado (EPCMs) foram construídos com a imobilização dos materiais sintetizados para a análise de Cu<sup>2+</sup>. O eletrodo modificado pela imobilização do material mesoporoso R2 (MCPE/R2) apresentou melhor sensibilidade para detecção de Cu<sup>2+</sup>. Em condições experimentais otimizadas, o MCPE/R2 apresentou comportamento linear entre 0,99 e 11,80 μmol L<sup>-1</sup>, sensibilidade com base no Limite de Detecção (LOD) de 0,50 μmol L<sup>-1</sup> e Limite de Quantificação (LOQ) de 0,99 μmol L<sup>-1</sup>, precisão (DPR<sub>máx</sub>) igual a 10,6% e recuperação de 92,2%. O desenvolvimento do método provou ser eficiente para a determinação de Cu<sup>2+</sup> em cachaça de cana de açúcar e a precisão dos resultados foram comparáveis aos obtidos por AAS.

Palavras-chave: Detecção eletroquímica, cobre, cachaça de cana de açúcar.

## 1. INTRODUCTION

Mesoporous silica has physical-chemical properties that can be modified to be applied in several research areas [1]. Modifications of these materials can be carried out by direct (hydrothermal or non-hydrothermal) methods and indirect (post-synthesis) methods such as aqueous impregnation, ion exchange of the driver and immobilization. The use of direct synthesis has many advantages, including better control of loads and more homogeneous distribution of functional groups [2, 3]. Modifications of mesoporous silica with amine functional group are one of the most widely used approach, specially due its many applications, which include catalysis, coupling and immobilization of functional molecules and biomolecules, drug delivery, synthesis of nanoparticles, adsorption of metal ions [4] and others.

Copper is an essential element for living organisms, but in excess, it can cause renal and hepatic disorders in humans and it is usually associated with neurodegenerative diseases such as Alzheimer and Parkinson [5, 6]. Copper is also known to be present in sugar cane spirit, a brazilian alcoholic beverage, obtained by the fermentation of sugarcane juice. Its production usually involves the use of copper stills, making the final product more susceptible to contamination by  $\text{Cu}^{2+}$ . Brazilian legislation determines the limit of  $5.0 \text{ mg L}^{-1}$  of copper in sugar cane spirit while international legislation determines lower limits ( $2.0 \text{ mg L}^{-1}$ ) [7, 8]. In this context, the search for sensitive, portable, versatile, and low-cost technique to analyze traces of copper ions is necessary [9]. Usually  $\text{Cu}^{2+}$  is analyzed by atomic absorption and inductively coupled plasma mass spectroscopy, but these methods, although sensitive, are expensive and require special pre-treatment of the sample [10, 11]. Among the new methods suggested in the literature, such as resonance, calorimetry, fluorescence, raman scattering and optical sensors, the electrochemical sensors arise as a promising alternative, since they are sensitive and selective as conventional methods, in addition to ease operation and capacity of miniaturization [12].

In the development of an electrochemical sensor, the sensitivity and selectivity is improved by the choice of the modifying material. Thus, it is expected that this specific material will improve the electrode to trigger, either by electrostatic attraction or complexation, a redox reaction. For copper detection, the use of various materials such as functionalized polymers, drugs, fibers and silicas immobilized on carbon paste electrodes have been studied [13-16]. The literature reports a series of functionalized mesoporous materials for the removal and detection of copper ions as well as the development of new optical and electrochemical sensors [17-19]. The use of mesoporous material functionalized with 3-aminepropyltriethoxysilane (APTS) and 3-aminepropyltrimethoxysilane (APMS) improve the efficiency of these materials for the detection of trace metals, specially copper, due chelating ability of the amine groups present on them. However, the functionalization is less common [4]. In this paper, we have successfully prepared a  $\text{Cu}^{2+}$  sensor based on modified carbon paste electrodes with mesoporous silica obtained through different synthetic routes.

## 2. EXPERIMENTAL SECTION

### 2.1 MATERIALS

Graphite powder and copper(II) nitrate hydrate were purchased from Aldrich. Potassium ferricyanide ( $\text{K}_3[\text{Fe}(\text{CN})_6]$ ) was purchased from J. T. Baker. Dibasic sodium phosphate dodecahydrate ( $\text{Na}_2\text{HPO}_4 \cdot 12\text{H}_2\text{O}$ ), anhydrous monobasic sodium phosphate ( $\text{NaH}_2\text{PO}_4$ ) were purchased from Synth. Ammonium chloride ( $\text{NH}_4\text{Cl}$ ), acetic acid ( $\text{CH}_3\text{COOH}$ ) were purchased from Vetec. Ammonium hydroxide ( $\text{NH}_4\text{OH}$ ) was purchased from Merck. Sodium acetate trihydrate ( $\text{Na}(\text{CH}_3\text{COO})_2 \cdot 3\text{H}_2\text{O}$ ) was purchased from Reagen. Ultrapure water was obtained from deionized water using an ultrapure water generator device, Millipore.

### 2.2 SYNTHESIS

*Synthesis of mesoporous silica (R1)*

The reagents used in the synthesis were silica gel, sodium silicate, hexadecyltrimethylammonium bromide (CTMABr) and distilled water [4, 20]. For the pH adjustment, 30% of acetic acid was used. The reagents were mixed in order to obtain a gel with the following molar composition:  $4.58\text{SiO}_2:0.44\text{Na}_2\text{O}:1.00\text{CTMABr}:200\text{H}_2\text{O}$ . The pH was adjusted in the range of 9.5 to 10. The synthesized gel was placed in a teflon-lined autoclave and heated to 140 °C for 24 hours. After this, the white precipitate was recovered by filtration, washed with water and drying at 100 °C for 2 hours. The CTMABr surfactant was removed by calcination at 450 °C for 2 hours using a ramp rate of 10 °C min<sup>-1</sup>.

#### *Mesoporous silica functionalization (R1)*

The functionalization of mesoporous silica was performed by the adsorption method adapted from the literature [4]. Briefly, 0.50 g of the calcined mesoporous silica was added to a mixture of 0.94 mmol of toluene and 2.40 mmol of APMS and stirred 4 h at ambient temperature. The product was filtered under vacuum and washed with toluene and dichloromethane, allowing to stand for several minutes until dryness. Finally, the fine powder was transferred to a vacuum desiccator in order to remove any residual solvent.

#### *Synthesis of mesoporous silica (R2)*

For this synthetic route, the mesoporous silica was functionalized in situ with APMS during the mesoporous structure formation [21]. The molar composition of the reagents used was  $0.10\text{CTMABr}:0.25\text{Na}_2\text{O}:1.00\text{SiO}_2:20.00\text{H}_2\text{O}:0.10\text{APMS}$ . Once mixed, the solution was stirred to obtain the final gel. The product was filtered under vacuum and washed with a mixture of hydrochloric acid:hexane (1:1) and heated to 70 °C in order to remove the driver from the pores of the material.

#### *Synthesis of mesoporous silica (R3)*

The synthesis was adapted from Iliade et al. (2012) [22]. Briefly, the mesoporous material was functionalized in situ and the reagents used in the synthesis were TEOS, sodium hydroxide, CTMABr, APMS and distilled water. The molar composition of the synthesis was  $0.002\text{CTMABr}:2.00\text{Na}_2\text{O}:0.018\text{SiO}_2:18.67\text{H}_2\text{O}:0.002\text{APMS}$ . The mixture was stirred for 2 hours at 80 °C. The precipitate formed was vacuum filtered and washed with distilled water and methanol, and then dried under vacuum at room temperature. The template was removed by ultrasonic scattering in ethanolic HCl solution. The obtained mesoporous was dried under vacuum at room temperature.

#### *Instrumentation*

X-ray were carried out in a Bruker (D8 Advance) X-ray equipment using Cu-K $\alpha$  radiation in 2 $\theta$  angle of 1 to 10°. Shimadzu (IR Prestige-21) FTIR spectrometer was used to obtain the IR spectra of all silicain the range of 4000 to 400 cm<sup>-1</sup>. The thermogravimetric curves were obtained in a TGA-50 Shimadzu using nitrogen as carrier gas at 40 mL min<sup>-1</sup>. The samples were heated from room temperature up to 900 °C, at 10 °C min<sup>-1</sup>. Nitrogen adsorption-desorption isotherms were performed at 77 K by using a ASIQM000-4 Quantachrome superficial area analyzer to determinate physical properties such as pore diameter, pore volume, pore wall thickness and surface area. The specific surface area was calculated using the Brunauer-Emmett-Teller (BET method) and pore size distributions from the branch adsorption isotherms by Barrett-Joyner-Halenda (BJH) method.

Pore wall thicknesses (W<sub>t</sub>) were estimated using  $W_t = [a_0 - D_p]$  ( $a_0$  = Mesoporous parameters, nm;  $D_p$  = Diameter pore, nm). The electrochemical measurements were carried using a Autolab 100 Potentiostat/Galvanostat. Differential pulse and stripping voltammetric experiments were performed in a one-compartment cell, using a carbon paste as working electrode, a platinum wire as auxiliary electrode and Ag/AgCl as reference electrode. The experiments were performed at 25 ± 1 °C. The pH value of aqueous solutions were buffered (pH 4.0 – 9.0).

### Modified electrodes

Unmodified carbon paste electrodes containing 7:3 by weight of carbon powder: mineral oil were used for comparison purpose. The modified carbon paste electrodes were prepared daily according to the mass ratio between carbon powder (graphite + modifier) and mineral oil (7:3) (Table 1). The mixture was subjected to mechanical maceration for 20 min in an agate mortar, obtaining a homogeneous mixture. The carbon paste mixture holder was constructed using a thick-walled glass tube with 0.10 cm internal diameter. A copper sleeve equipped with a copper wire plunger was mounted at the top of the glass tube. By rotating the sleeve, the plunger extruded the used paste layer which was sliced off and a fresh paste surface was formed and hand-polished on a weighing paper.

Table 1. Modified carbon paste electrodes.

	Synthetic route	Abbreviation
	R1	MCPE/R1 <sub>a</sub>
Modified electrodes	R1-funcionalized	MCPE/R1 <sub>b</sub>
	R2-funcionalized	MCPE/R2
	R3-funcionalized	MCPE/R3

### Analytical procedure

A stock solution of hydrate cooper (II) nitrate (10 mmol L<sup>-1</sup>) was prepared and aliquots were diluted with phosphate buffer solution (pH 6.0) to obtain the concentration range of 0.99 up to 11.9 μmol l<sup>-1</sup>. The Cu<sup>2+</sup> determinations using electrodes with different silicas were carried out by stripping voltammetric analysis. All measurements were performed at room temperature.

### Sugar Cane Spirit Samples

The sample of sugar cane spirit (“cachaça”) was acquired from artisanal producers from Sergipe state. The ratio 9.5:0.5 (phosphate buffer:sugar cane spirit) was used to determine copper ions in the sugar cane spirit samples.

## 3. RESULTS AND DISCUSSION

### 3.1 CHARACTERIZATION OF MESOPOROUS SILICA MATERIALS

Table S1 and Figure S1 show the main bands observed in the FTIR spectra for the mesoporous silicas (R1<sub>a</sub>) and for the materials modified with APMS (R1<sub>b</sub>, R2 and R3). The bands around 1080, 790 and 460 cm<sup>-1</sup> present in all samples are typical Si-O-Si bonds, attributed to the condensed silica network [23]. The band around 1640 cm<sup>-1</sup> is mainly from the bending vibration of adsorbed water. The materials exhibited a band in 960 cm<sup>-1</sup>, which was assigned to the symmetric stretching vibration of the Si-OH groups. The hydroxyl groups on mesoporous structure also appear at 3466-3442 cm<sup>-1</sup> range. It is observed that the CTMA<sup>+</sup> was fully removed from the mesoporous structure due the vibration bands in 2930-2854 cm<sup>-1</sup> range, typical of C-H stretching bonds of CH<sub>2</sub> and CH<sub>3</sub> groups on CTMA<sup>+</sup> species. It is also observed at 1487 cm<sup>-1</sup> the asymmetric deformation of methyl group (CH<sub>3</sub>-N<sup>+</sup>) disappearing after calcinations process [24]. The bands around 1555 and 693 cm<sup>-1</sup> are attributed to NH deformation bond, evidencing the process of functionalization of the mesoporous silica [25]. Other evidence that the APMS was added to the mesoporous structure is the presence of the low intensity band around 2943 cm<sup>-1</sup>, attributed to the C-H (sp<sup>3</sup> carbon) stretch of the propyl group [4].

Figure 1 shows the isotherms obtained for the mesoporous silicas. They can be assigned as type IV, characteristic of mesoporous materials according to IUPAC classification. At low relative pressures, P/P<sub>0</sub> < 0.2, a monolayer coverage is expected. The sharp inflections in P/P<sub>0</sub> around 0.3

are characteristic of uniform capillary condensation, indicating the presence of ordered mesoporous. The horizontal hysteresis loop after  $P/P_0 = 0.45$  suggests the existence of mesoporous secondary texture and the increase in nitrogen adsorption from  $P/P_0 = 0.8$  indicates the presence of larger pores and its pore size distribution is rather broad [26]. The specific surface area ( $S_{\text{BET}}$ ), pore volume ( $V_p$ ), pore wall thicknesses ( $W_t$ ) and pore diameter ( $D_p$ ) values are typical for these mesoporous silica (Table 2). After functionalization with APMS, the  $N_2$  adsorption-desorption isotherms demonstrate a significant change in the profile, indicating that the materials lose their initial textural characteristics. A significant reduction in the surface area and pore volume were observed, probably due to the almost complete filling of the pores with amine functional groups. Similar results were found by Liu et al (2016), working with highly hydrophobic MCM-41 mesoporous molecular sieves [27].

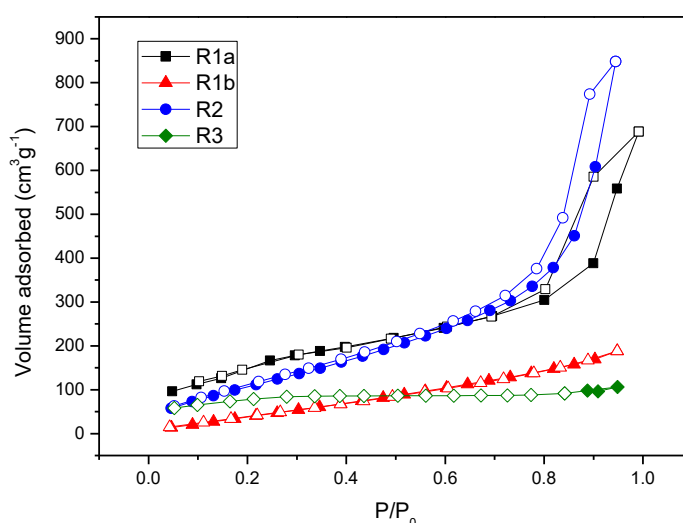


Figure 1. Adsorption/desorption isotherms for synthesized mesoporous materials.

Table 2. Textural properties of mesoporous silicas.

Materials	$S_{\text{BET}}$ ( $\text{m}^2 \text{g}^{-1}$ )	$V_p$ ( $\text{cm}^3 \text{g}^{-1}$ )	$D_p$ (nm)	$W_t^*$
R1a	187.05	0.28	3.60	1.05
R1b	158.17	0.26	3.30	1.35
R2	430.53	1.28	3.64	-
R3	11.88	0.05	1.93	-

$$* W_t = a_0 - D_p$$

The mesoporous silica R1a (Figure S2) X-ray analysis is characteristic of a material with hexagonal channel order, which is consistent with that obtained by Beck et al. [28]. The MCM-41 material is characterized by five diffraction peaks, referring to the index planes (100), (110), (200), (210) and (300), which indicates how the material is ordered, where the planes (100) (110) and (200) are the most important. [28, 29]. The mesoporous silica R1b X-ray diffraction profile has changed after adding the APMS (Figure S2). The peaks intensities decreased significantly and were shifted to higher  $2\theta$  angles. However, the more intense diffraction peak in  $2.18^\circ$  for mesoporous silicas R1b still remained, indicating the preserved meso-channel structure after the introduction of amine groups. The diffractograms of the functionalized materials from the second and third synthetic routes did not reveal any evidence of MCM-41 mesostructures plane formation, although the surface areas and pore diameters are characteristic of mesoporous silica. The Thermogravimetric (TG) analysis have showed the following stages: desorption of intracrystalline water; decomposition of the amine group and decomposition of the template strongly bond to the surface (Figure S3 and Table S2). As shown in Figure S3, the mesoporous silica R1a has two mass loss, one in between 30 and 100 °C and one from 100 to 600 °C. These

events of mass loss can be attributed to desorption of physically and chemically adsorbed water, respectively [30]. TG curves for R1b, R2 and R3 mesoporous materials show three different mass loss regions: the first from 30 to 100°C refers to desorption of physically adsorbed water; the second from 100 to 400 °C attributed to desorption of physically adsorbed amine; and the third from 400 to 700 °C due residual amine decomposition which is more strongly linked and due to the loss of silanol groups [30, 31]. This result show that the maximum temperature that the R1b, R2 and R3 materials should be lower than 100°C, because above this, the decomposition of the APMS begins to occur.

### 3.2 ANALYTICAL CHARACTERISTICS OF MODIFIED ELECTRODES

The electrochemical behavior of MCPE/R2 was investigated in the presence of  $K_3[Fe(CN)_6]$  in KCl 0.1 mmol L<sup>-1</sup>. It revealed a linear correlation between the square root of scan rates ( $v^{1/2}$ ) versus peak currents (Figure 2) and a characteristic behavior of reversible electrochemical processes with diffusional control. An average effective area of 0.0308 cm<sup>2</sup> was obtained, which is higher than the geometric area (0.0078 cm<sup>2</sup>), resulting in a greater electrode- analyte interaction and enhancing the current signals, according to Randles-Sevcik equation [32].

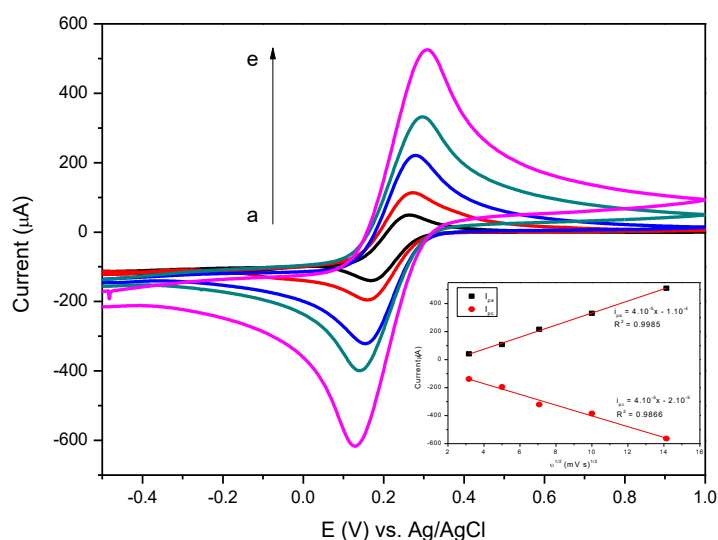


Figure 2. Cyclic voltammograms of MCPE/R2 in presence of 50 mmol L<sup>-1</sup>  $[Fe(CN)_6]^{3-/4-}$  in 0.1 mol L<sup>-1</sup> KCl solution at different scan rates (a → e). Inset: Relationship between square root of scan rates ( $v^{1/2}$ ) versus peak currents.

The above mentioned comparative study evaluated the voltammetric profiles of Cu<sup>2+</sup> ions obtained by unmodified carbon paste electrodes and its modified version with 10% of mesoporous materials. MCPE/R1<sub>a</sub> have showed a broad oxidation signal in the absence of Cu<sup>2+</sup>, which overlaps with the analyte oxidation signals (Figure S4), indicating that MCPE/R1<sub>a</sub> is not sufficiently selective for copper determinations. The copper was electroactive for all othersmodified electrodes, generating an oxidation peak (Cu<sup>0</sup>/Cu<sup>2+</sup>) at +0.1 V (Ag/AgCl) (Figure 3). The decrease of MCPE/R3 signal intensity suggests that the high hygroscopy of the material plays an important role in the carbon paste conductivity. For MCPE/R1<sub>b</sub> and MCPE/R2, an increase in the analytical signals was observed. This behavior may be associated with the presence of the amine groups, which has the ability to coordinate with copper ions. Parida et al. (2012) have attributed this behavior to the presence of amine groups in the electrode surface [33]. The MCPE/R2 was chosen for later studies, since it have showed better analytical signal and sensitivity for the detection of copper ions.

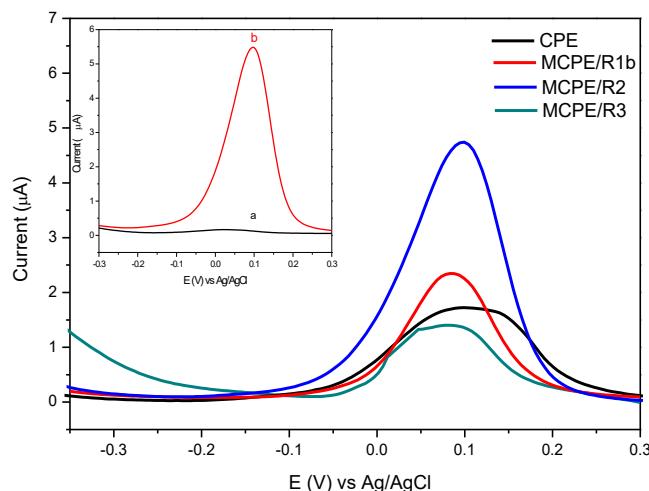


Figure 3. Anodic stripping differential pulse voltammograms of carbon paste electrode (CPE) and carbon paste electrode modifieds (MCPEs) in the presence of  $1.0 \times 10^{-4} \text{ mol L}^{-1}$  of  $\text{Cu}^{2+}$ . Inset: Anodic stripping differential pulse voltammograms of MCPE/R2 a) blank, b)  $1.0 \times 10^{-4} \text{ mol L}^{-1}$   $\text{Cu}^{2+}$ . The experimental conditions were phosphate buffer (pH 6.0), accumulation potential  $-0.3 \text{ V}$  for 300 s and scan rates of  $10 \text{ mV s}^{-1}$ .

### 3.3 OPTIMIZATION OF EXPERIMENTAL PARAMETERS AT MCPE/R2

The optimization of an electrochemical methodology is very important in order to improve the analytical response profile. The stripping peak current is pH dependent, showing its maximum at  $\text{pH} = 6$  (Figure 4). This behavior may be explained by the presence of protons and its influence on amino-group chelating ability. The lack of  $\text{H}^+$  ( $\text{pH} > 6$ ) favors the the desorption of copper in the oxidation stage, while the excess of  $\text{H}^+$  ( $\text{pH} < 6$ ) leads to the competition of  $\text{H}^+$  and  $\text{Cu}^{2+}$  ions during the adsorption step, reducing the detection of copper ions [35]. The anodic peak current obtained in alkaline media is justified by the presence of hydroxyl ions in solution, leading to the formation of  $\text{Cu}(\text{OH})_2$  [36, 37].

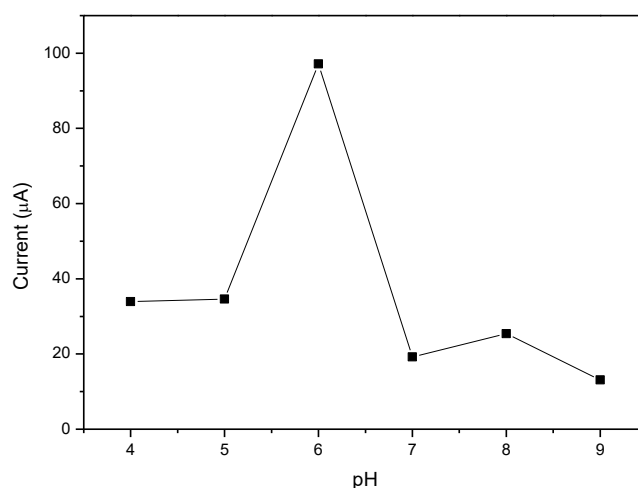


Figure 4. Variation of the anodic peak currents as a function of pH in presence  $1.0 \times 10^{-4} \text{ mol L}^{-1}$   $\text{Cu}^{2+}$  in MCPE / R2<sub>10%</sub>. Conditions: scan rates  $10 \text{ mV s}^{-1}$ , pre-concentration potential  $-0.5 \text{ V}$  for 300 s.

The electrode composition was evaluated in the range of 0 to 25% (m/m). The peaks currents increased with the increasing of mesoporous silica amount up to 15% (Figure S5) and decreased after that due to a decrease in the graphite content in the paste and reduction of the electrode area

conductivity [33, 34]. The assessment of the pre-concentration potential (-0.2 to -0.7 V) indicates that -0.5 V was sufficient to promote the reduction of copper ions (Figure 5). Pre-concentration time (0.5 to 15 minutes) showed an increase of the stripping peak current up to 10 minutes of pre-concentration, above that time, no significant differences were found (Figure S6). The variation of stripping peak current as a function of the scan rates (5 to 50  $\text{mV s}^{-1}$ ) was not significant, however, it was observed a widening in the voltammetric profile when using scan rates greater than 20  $\text{mV s}^{-1}$ . Within this context, 10  $\text{mV s}^{-1}$  was determined as the ideal scan rates for the present study.

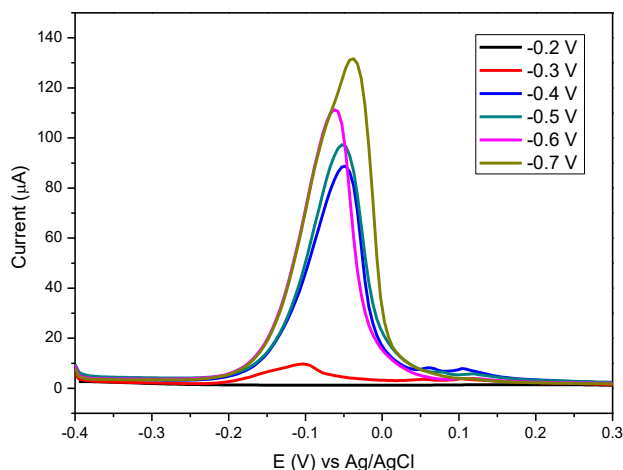


Figure 5. Anodic stripping differential pulse voltammograms of MCPE/R2<sub>10%</sub> in presence  $1.0 \times 10^{-4} \text{ mol L}^{-1} \text{ Cu}^{2+}$  varying pre-concentration potential for 600 s. Conditions: phosphate buffer pH 6.0 and scan rates  $10 \text{ mV s}^{-1}$ .

### 3.4 ANALYTICAL PERFORMANCE OF SENSOR

The analytical curve obtained by the standard addition method under optimized conditions (Figure 6) revealed that linearity of anodic stripping peak currents increase as  $\text{Cu}^{2+}$  concentrations increases from 0.99 to  $11.80 \text{ μmol L}^{-1}$ . The linear regression equation is described by  $I_{pa} = 3.106 [\text{Cu}^{2+}] - 9.079 \times 10^{-7}$ , with  $R^2 = 0.995$  for  $n = 8$  and  $\text{LOD} = 0.50 \text{ μmol L}^{-1}$  and  $\text{LOQ} = 0.99 \text{ μmol L}^{-1}$ .

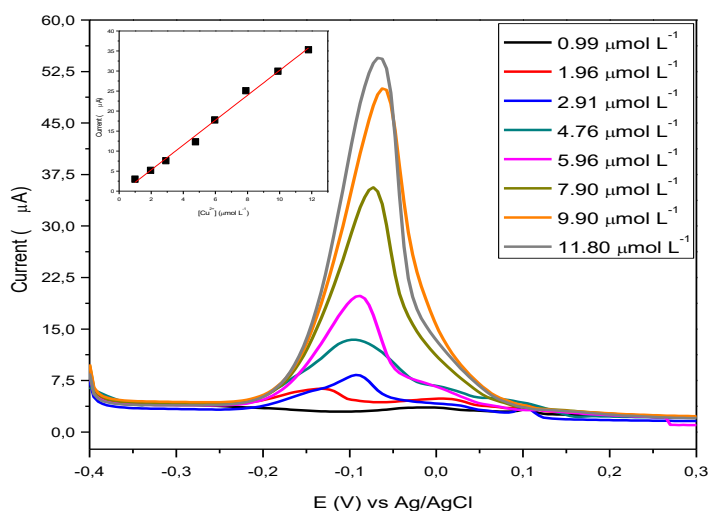


Figure 6. Anodic stripping differential pulse voltammograms of MCPE/R2<sub>10%</sub> in the detection of different concentrations of  $\text{Cu}^{2+}$ . Conditions: phosphate buffer pH 6.0; scan rate  $10 \text{ mV s}^{-1}$ , pre-concentration potential -0.5 V for 600 s. Inset: analytical curve.

The relative standard deviation (RSD) and recovery of the method were evaluated by means in nine samples at three concentrations of  $\text{Cu}^{2+}$  (2.91, 5.96 and 11.80  $\mu\text{mol L}^{-1}$ ) in triplicate [38]. The RSD values (7.00, 10.62 and 7.10%) were satisfactory, since 20% is the usual limit for trace elements determinations [39]. Recovery levels of 92.24%, 93.99% and 93.20% for the three concentrations were also acceptable, taking into account the range established by ANVISA (70 - 120%) and in agreement with what have been reported for electrochemical methods (over 90%) [40-41]. The selectivity of the proposed method was also investigated in a range of 0.1:1, 1:1, 10:1 ( $M^{2+}:\text{Cu}^{2+}$ ) proportions (Table S3) [35, 42-43]. The interference of the ions follows the order  $\text{Pb}^{2+} > \text{Mn}^{2+} > \text{Zn}^{2+} > \text{Cd}^{2+} > \text{Fe}^{2+}$  and presents higher interference with lead ions that can be justified by competition with copper ions (Figure 7) and the preference to coordinate to  $\text{RNH}_2$  groups. The matrix effect was evaluated and the ration  $a_{\text{matrix}}/a_{\text{solvent}}$  was equal to 1.1 ( $> 1$ ), indicating that the matrix effect in the voltammetric response is positive, resulting in a slightly increase of signal [44]. In order to minimize the matrix effect, it was decided to electrochemically quantify  $\text{Cu}^{2+}$  ions through the curve using the matrix itself.

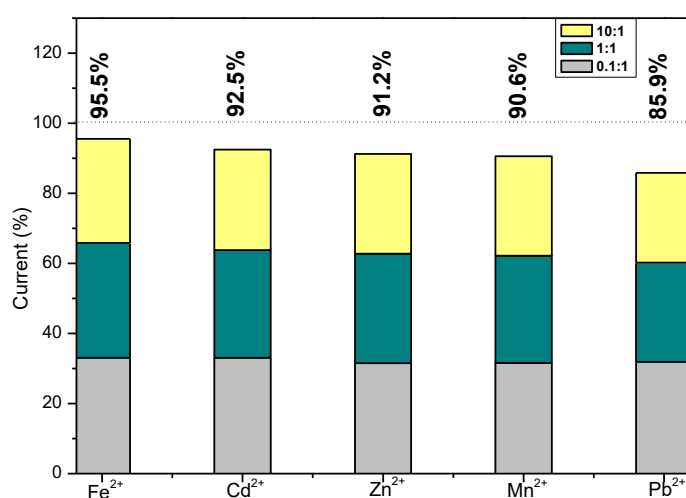


Figure 7. Variation of the anodic peak currents of the determination of  $\text{Cu}^{2+}$  using MCPE/ R2<sub>10%</sub> in the presence of interferents ( $M^{2+}$ ).

### 3.5 DETERMINATION OF $\text{Cu}^{2+}$ IONS IN REAL SAMPLES

The electrochemical signal of  $\text{Cu}^{2+}$  in sugar cane was observed by the increase of the anodic peak currents around -0.1 V and its quantification was done by the standard addition method.. An amount of 0.90  $\mu\text{mol L}^{-1}$  of  $\text{Cu}^{2+}$  was determined by extrapolating the calibration curve (Figure 8), described by  $I_{\text{pa}} = 3.31 [\text{Cu}^{2+}] - 3.00 \times 10^{-6}$ ,  $R^2 = 0.995$  (Figure 8). The value was comparable with the results obtained by flame atomic absorption spectroscopy (FAAS) (0.94  $\mu\text{mol L}^{-1}$ ). The anodic stripping voltammetric method using modified electrode MCPE/R2 indicated that the analyzed sample contains 1.14  $\text{mg.L}^{-1}$  of copper, which is lower than the limit established by the Brazilian resolution (5.0  $\text{mg L}^{-1}$ ).

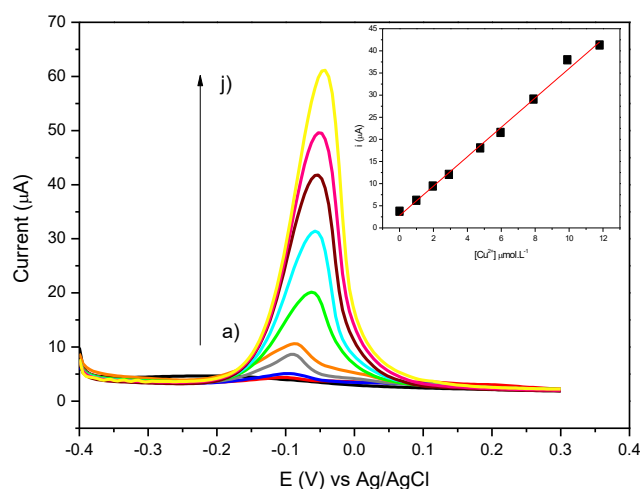


Figure 8. Anodic stripping differential pulse voltammograms of MCPE/R2<sub>10%</sub> in different concentrations of Cu<sup>2+</sup>. a) blank, b) 5% sugar cane spirit. Conditions: 5% sample, 95% phosphate buffer pH 6.0 and scan rates 10 mV s<sup>-1</sup>, pre-concentration potential -0.5 V for 600 s. Inset: variation of the anodic peak current at the 0.08 V potential as a function of the Cu<sup>2+</sup> concentrations.

#### 4. CONCLUSIONS

The proposed routes were able to synthesize functionalized mesoporous silica matrices with pore sizes within the IUPAC established for this classification. It was observed that the high surface area of the mesoporous silica showed a higher sensitivity for the electrochemical detection of Cu<sup>2+</sup> by differential pulse anodic stripping voltammetry (DPASV). The method developed with a linear range of 0.99 to 11.80 µmol L<sup>-1</sup> ( $R^2 = 0.995$ ) showed acceptable precision (RSD<sub>max</sub> = 10.6%), recovery 92.2%, LOD = 0.50 µmol L<sup>-1</sup> and LOQ = 0.99 µmol L<sup>-1</sup>. The electrochemical detection of copper(II) using MCPE/R2<sub>10%</sub> was efficient for the analysis of sugar cane spirit samples, since the Cu<sup>2+</sup> content obtained for the artisanal sample was comparable to that obtained by AAS.

#### 5. ACKNOWLEDGEMENTS

Authors are grateful to Brazilian funding agencies CNPq, CAPES and FAPITEC/SE for financial support.

#### 6. REFERENCES

1. Chen C, Kim J, Ahn WS. CO<sub>2</sub> capture by amine-functionalized nanoporous materials: A review. *Korean J Chem Eng.* 2014;Nov:31(11):1919-1934, doi:10.1007/s11814-014-0257-2.
2. Ortiz-Bustos J, Martín A, Morales V, Sanz R, García-Munoz RA. Surface-functionalization of mesoporous SBA-15 silica materials for controlled release of methylprednisolone sodium hemisuccinate: Influence of functionality type and strategies of incorporation. *Microporous Mesoporous Mater.* 2017;Mar:240:236-245, doi: 10.1016/j.micromeso.2016.11.021.
3. Soltani S, Rashid U, Al-Resayes SI, Nehdi IA. Recent progress in synthesis and surface functionalization of mesoporous acidic heterogeneous catalysts for esterification of free fatty acid feedstocks: A review. *Energy Convers Manag.* 2017;June:141:183–205, doi: 10.1016/j.enconman.2016.07.042.
4. Santos DO, Santos MLN, Costa JAS, Jesus RA, Navickene S, Sussuchi EM, Mesquita ME. Investigating the potential of functionalized MCM-41 on adsorption of Remazol Red dye. *Environ Sci Pollut Res.* 2013;Jan:20(7):5028-5035, doi:10.1007/s11356-012-1346-6.
5. Su J, Xu J, Chen Y, Xiang Y, Yuan R, Chai Y. Sensitive detection of copper (II) by a commercial glucometer using click chemistry. *Biosens Bioelectron.* 2013;Jan:45:219–222, doi:10.1016/j.bios.2013.01.069.

6. Tang L, Wang N, Zhang Q, Guo J, Nandhakumar R. A new benzimidazole-based quinazoline derivative for highly selective sequential recognition of  $\text{Cu}^{2+}$  and  $\text{CN}^-$ . *Tetrahedron Lett.* 2013;Feb:54(6):536–540, doi: 10.1016/j.tetlet.2012.11.078.
7. Pasquini C, Filho BBF. Mechanization of measurement of laser induced breakdown spectroscopy/ring-oven pre-concentration: determination of copper in cachaça. *Anal Methods.* 2016;Jan:8(40):7354–7360, doi: 10.1039/C6AY01555G.
8. Zacaroni LM, Magriotis ZM, Cardoso M das G, Santiago WD, Mendonça JG, Vieira SS, Nelson DL. Natural clay and commercial activated charcoal: Properties and application for the removal of copper from cachaça. *Food Control.* 2015;July:47:536–544, doi: 10.1016/j.foodcont.2014.07.035.
9. Bouden S, Bellakhal N, Chaussé A, Dachraoui M, Vautrin-UI C. Correlations between the grafting conditions and the copper detection by diazonium functionalized carbon screen-printed electrodes. *Electrochim Acta.* 2014;Jan:125:149–155, doi: 10.1016/j.electacta.2014.01.083.
10. Yoon JW, Chang MJ, Hong S, Lee MH. A fluorescent probe for copper and hypochlorite based on rhodamine hydrazide framework. *Tetrahedron Letters.* 2017;Aug:58(40):3887–3893, doi: 10.1016/j.tetlet.2017.08.071.
11. Su J, Xu J, Chen Y, Xiang Y, Yuan R, Chai Y. Sensitive detection of copper (II) by a commercial glucometer using click chemistry. *Biosens Bioelectron.* 2013;Jan:45:219–222, doi: 10.1016/j.bios.2013.01.069.
12. Bai J, Chen Y, Li P, Sun D, Tang Y. *J. Electroanal. Chem.* 2015;754:1–7.
13. Janegitz BC, Marcolino-Junior LH, Campana-Filho SP, Faria RC, Fatibello-Filho O. Anodic stripping voltammetric determination of copper(II) using a functionalized carbon nanotubes paste electrode modified with crosslinked chitosan. *Sensors Actuators B Chem.* 2009;Aug:142(1):260–266, doi: 10.1016/j.snb.2009.08.033.
14. Zhihua W, Xiaole L, Jianming Y, Yaxin Q, Xiaoquan L. Copper(II) determination by using carbon paste electrode modified with molecularly imprinted polymer. *Electrochim Acta.* 2011;Oct:58:750–756, doi: 10.1016/j.electacta.2011.10.034.
15. Ashrafi AM, Vytřas K. New procedures for voltammetric determination of copper (II) using antimony film-coated carbon paste electrodes. *Electrochim Acta.* 2012;Dec:73:112–117, doi: 10.1016/j.electacta.2011.12.042.
16. Nezhadali A, Sadeghzadeh S. Optimization of stripping voltammetric sensor by mixture design-artificial neural network genetic algorithm for determination of trace copper(II) based on iodoquinol-carbon nanotube modified carbon paste electrode. *Sens Actuators B.* 2016;Mar:224:134–142, doi: 10.1016/j.snb.2015.09.154.
17. Behbahani M, Najafi F, Amini MM, Sadeghi O, Bagheri A, Hassanlou PG. Solid phase extraction using nanoporous MCM-41 modified with 3,4-dihydroxybenzaldehyde for simultaneous preconcentration and removal of gold(III), palladium(II), copper(II) and silver(I). *J Ind Eng Chem.* 2014;Sep:20(4):2248–2255, doi: 10.1016/j.jiec.2013.09.057.
18. Saleh SM, Ali R, Ali IAL. A novel, highly sensitive, selective, reversible and turn-on chemisensor based on Schiff base for rapid detection of Cu(II). *Spectrochim Acta. Part A.* 2017;Apr:183:225–231, doi: 10.1016/j.saa.2017.04.019.
19. Santos JC, Matos CRS, Pereira GBS, Santana TBS, Souza HO, Costa LP, Sussuchi EM, Souza AMGP, Gimenez IF. Stable CdTe nanocrystals grown in situ in thiol-modified MCM-41 mesoporous silica: Control synthesis and electrochemical detection of  $\text{Cu}^{2+}$ . *Microporous Mesoporous Mater.* 2016;Sep:221:48–57, doi: 10.1016/j.micromeso.2015.09.024.
20. Santos SCG, Machado SWM, Garrido Pedrosa AM, Souza, MJB. Development of micro-mesoporous composite material of the ZSM-12/MCM-41 type for the  $\text{CO}_2$  adsorption. *J Porous Mater.* 2015;June:22(5):1145–1151, doi: 10.1007/s10934-015-9990-0.
21. Liu X, Du Y, Guo Z, Gunasekara S, Ching C-B, Chen Y, Leon SSJ, Yang Y. Monodispersed MCM-41 large particles by modified pseudomorphic transformation: Direct diamine functionalization and application in protein bioseparation. *Microporous Mesoporous Mater.* 2010;Feb:122:(1-3):114–120, doi: 10.1016/j.micromeso.2009.02.023.
22. Iliade P, Miletto I, Coluccia S, Berlier G. Functionalization of mesoporous MCM-41 with aminopropyl groups by co-condensation and grafting: a physico-chemical characterization. *Res Chem Intermed.* 2012;Mar:38(3-5):785–794, doi: 10.1007/s11164-011-0417-5.
23. Akondi AM, Trivedi R, Sreedhar B, Kantam M, Bhargava S. Cerium-containing MCM-41 catalyst for selective oxidative arene cross-dehydrogenative coupling reactions. *Catal Today.* 2012;June:198(1):35–44, doi: 10.1016/j.cattod.2012.05.029.
24. Dündar-Tekkaya E, Yürüm Y. Effect of loading bimetallic mixture of Ni and Pd on hydrogen storage capacity of MCM-41. *Int J Hydrogen Energy.* 2015;Mar:40(24):7636–7643, doi: 10.1016/j.ijhydene.2015.02.108.

25. Ayad MM, Salahuddin NA, El-Nasr AA, Torad NL. Amine-functionalized mesoporous silica KIT-6 as a controlled release drug delivery carrier. *Microporous Mesoporous Mater.* 2016;Apr:229:166-177, doi: 10.1016/j.micromeso.2016.04.029.
26. Thommes M, Kaneko K, Neimark AV, Olivier JP, Rodriguez-Reinoso F, Rouquerol J, Sing KSW. Physisorption of gases, with special reference to the evaluation of surface area and pore size distribution (IUPAC Technical Report). *Pure Appl Chem.* 2015;Apr:87(9-10):1051-1069, doi: 10.1515/pac-2014-1117.
27. Liu X, Hu Y, Huang J, Wei C. Detailed characteristics of adsorption of bisphenol A by highly hydrophobic MCM-41 mesoporous molecular sieves. *Res Chem Intermed.* 2016;Mar:42(9):7169-7183, doi: 10.1007/s11164-016-2526-7.
28. Beck JS, Vartuli JC, Roth WJ, Leonowicz ME, Kresge CT, Schmitt KD, Chu CT-W, Olson DH, Sheppard EW, McCullen SB, Higgins JB, Schlenker JL. A New Family of Mesoporous Molecular Sieves Prepared with Liquid Crystal Templates. *J Am Chem Soc.* 1992;June:114(27):10834-10843, doi: 10.1021/ja00053a020.
29. Li L, Wang X, Zhang D, Guo R, Du X. Excellent adsorption of ultraviolet filters using silylated MCM-41 mesoporous materials as adsorbent. *Appl Surf Sci.* 2015;Nov:328:26-33, doi: 10.1016/j.apsusc.2014.11.116.
30. Berlier G, Gastaldi L, Sapino S, Miletto I, Bottinelli E, Chirio D, Ugazio E. MCM-41 as a useful vector for rutin topical formulations: Synthesis, characterization and testing. *Int J Pharm.* 2013;Sep:457(1):177-186, doi: 10.1016/j.ijpharm.2013.09.018.
31. Rossetto E, Nicola B P, de Souza RF, Bernardo-Gusmão K, Pergher SBC. Heterogeneous complexes of nickel MCM-41 with b-diimine ligands: Applications in olefin oligomerization. *J Catal.* 2015;Dec:323:45-54, doi: 10.1016/j.jcat.2014.12.026.
32. Li Y, Jiang Y, Mo T, Zhou H, Li Y, Li S. Highly selective dopamine sensor based on graphene quantum dots self-assembled monolayers modified electrode. *J Electroanal Chem.* 2016;Apr:767:84-90, doi: 10.1016/j.jelechem.2016.02.016.
33. Parida K, Mishra KG, Dash SK. Adsorption of Copper(II) on NH<sub>2</sub>-MCM-41 and Its Application for Epoxidation of Styrene. *Ind Eng Chem Res.* 2012;Dec:51(5):2235-2246, doi: 10.1021/ie200109h.
34. Arvand M, Fallahi P. Voltammetric determination of rivastigmine in pharmaceutical and biological samples using molecularly imprinted polymer modified carbon paste electrode. *Sens Actuators* 201;July:188:797-805, doi: 10.1016/j.snb.2013.07.092.
35. Oliveira PR, Lamy-Mendes AC, Rezende EIP, Mangrich AS, Marcolino Junior LH, Bergamini MF. Electrochemical determination of copper ions in spirit drinks using carbon paste electrode modified with biochar. *Food Chem.* 2015;Sep:171:426-431, doi: 10.1016/j.foodchem.2014.09.023.
36. Mehta VN, Kumar MA, Kailasa SK. Colorimetric Detection of Copper in Water Samples Using Dopamine Dithiocarbamate-Functionalized Au Nanoparticles. *Ind Eng Chem Res.* 2013;Feb:52(12):4414-4420, doi: 10.1021/ie302651f.
37. Suguihiro TM, de Oliveira P R, de Rezende EIP, Mangrich AS, Marcolino Junior LH, Bergamini M F. An electroanalytical approach for evaluation of biochar adsorption characteristics and its application for Lead and Cadmium determination. *Biores Technol.* 2013;May:143:40-45, doi: 10.1016/j.biortech.2013.05.107.
38. National Health Surveillance Agency, [http://www.abrifar.org.br/novo/Site/anexos/CP\\_129\\_2016Minuta.pdf](http://www.abrifar.org.br/novo/Site/anexos/CP_129_2016Minuta.pdf), 2016. (accessed 02 August 2017).
39. Miranda L, Felsner ML, Torres YR, Hoss I, Galli A, Quinária SP. Validação intralaboratorial da determinação de metiltestosterona em águas naturais por voltametria usando eletrodo de gota pendente de mercúrio. *Quim Nova.* 2015 Feb;38(3):419-426, doi: 10.5935/0100-4042.20150014.
40. National Institute of Metrology, Quality and Technology, [http://www.inmetro.gov.br/Sidoq/Arquivos/CGCRE/DOQ/DOQ-CGCRE-8\\_05.pdf](http://www.inmetro.gov.br/Sidoq/Arquivos/CGCRE/DOQ/DOQ-CGCRE-8_05.pdf), 2016. (accessed 02 August 2017).
41. Sha R, Komori K, Badhulika S. Graphene-Polyaniline composite based ultra-sensitive electrochemical sensor for non-enzymatic detection of urea. *Electrochim Acta.* 2017;Mar:233:44-51, doi: 10.1016/j.electacta.2017.03.043.
42. National Institute of Metrology, Quality and Technology, <http://www.inmetro.gov.br/legislacao/rtac/pdf/RTAC001497.pdf>, 2009. (accessed 02 August 2017).
43. de Souza JC, Pezza HR, Pezza L. A simple and green analytical method for determination of copper(II) in whisky and sugarcane spirit by diffuse reflectance spectroscopy. *Anal Methods.* 2016;Feb:8(8):1867-1875, doi: 10.1039/c5ay03073k.
44. Pinho GP de, Silvério FO, Neves AA, Queiroz MELR, Starling MAVM. Influência dos constituintes químicos dos extratos de diferentes matrizes na resposta cromatográfica de agrotóxicos. *Quim Nova.* 2010;Mar:33(4):909-913, doi: 10.1590/S0100-40422010000400028.

### Supporting information

**Table S1.** Main bands observed in the FTIR spectra of the mesoporous silica.

Attributions	Wavenumber (cm <sup>-1</sup> )			
	R1a	R1b	R2	R3
v(Si-O-Si)	1093	1077	1081	1084
v(Si-O-Si)	794	786	794	797
v(Si-O)	465	458	461	461
v(Si-OH)	960	-	946	951
v(OH)	3447	3466	3450	3442
v(OH)	1641	1641	1623	1641
δ(NH)	-	1554	1511	1515
v(NH)	-	693	689	-

**Table S2.** Temperature range and respectively mass loss of the mesoporous silicas.

Attributions	Mass loss (%)			
	R1 <sub>a</sub>	R1 <sub>b</sub>	R2	R3
Water desorption	0.3	6.2	0.4	29.3
Template decomposition	-	-	4.0	4.1
APTS Decomposition	-	10.3	3.2	2.1
Hydrolysis Si-OH	3.6	2.1	0.5	2.0
<b>Total</b>	<b>3.9</b>	<b>18.6</b>	<b>7.7</b>	<b>37.6</b>

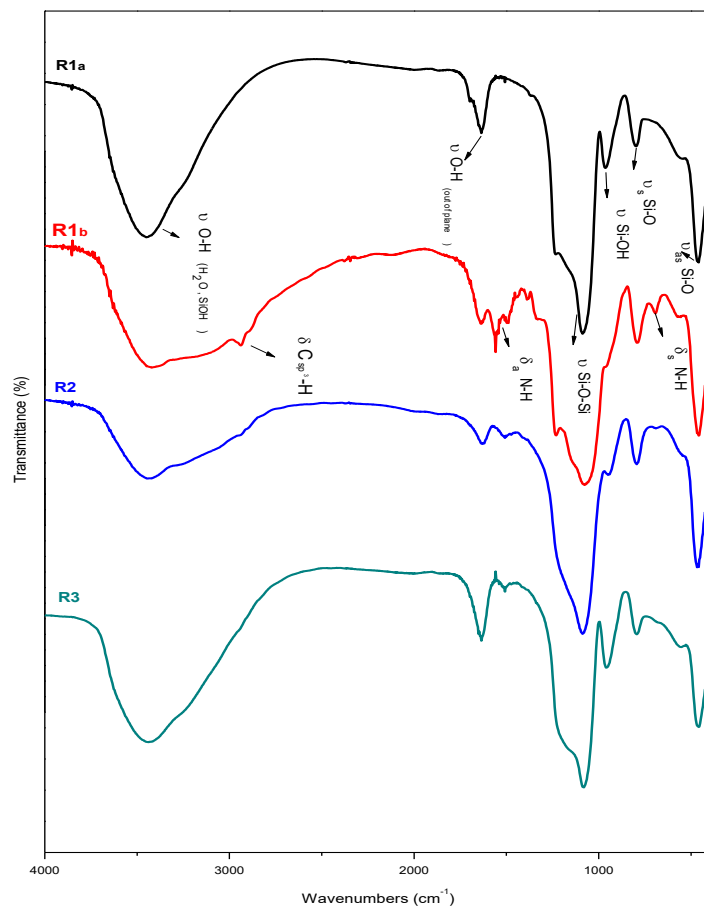


**Figure S1.** IR spectra of the mesoporous materials obtained by the first (R1<sub>a</sub> - unfunctionalized / R1<sub>b</sub> - functionalized), second (R2) and third (R3) synthetic routes.

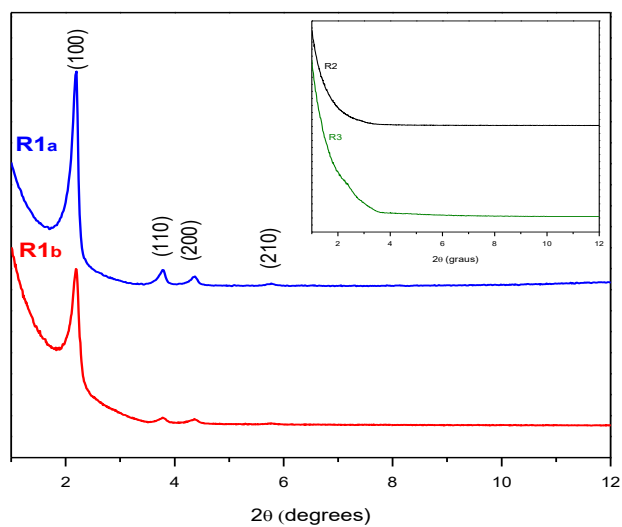


**Figure S2.** X-ray diffractograms of mesoporous silicas.

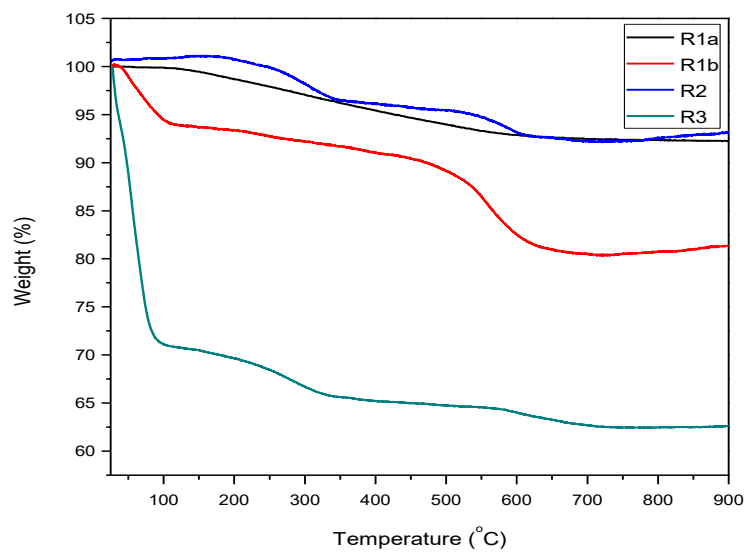


**Figure S3.** TG curves of the mesoporous silicas.

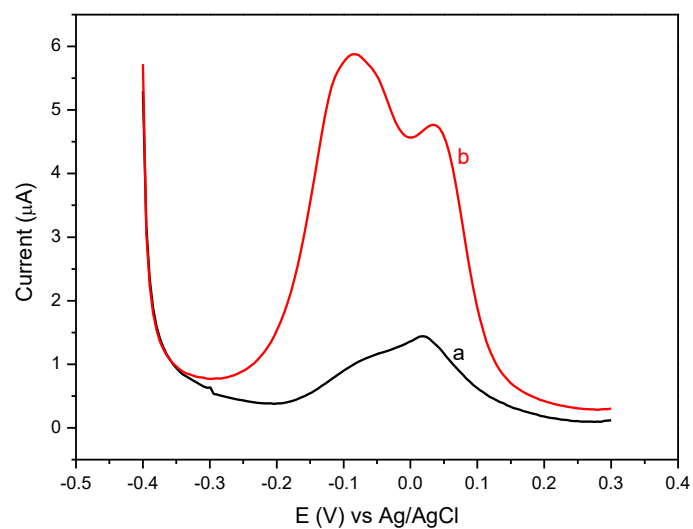


**Figure S4.** Anodic stripping differential pulse voltammograms of the MCPE R1<sub>a</sub>: (a) Absence of Cu<sup>2+</sup>, (b) 1 × 10<sup>-4</sup> mol L<sup>-1</sup> Cu<sup>2+</sup>. Conditions: ammonia buffer pH 9, scan rates 10 mV s<sup>-1</sup>, pre-concentration potential -0.3 V for 300 s.

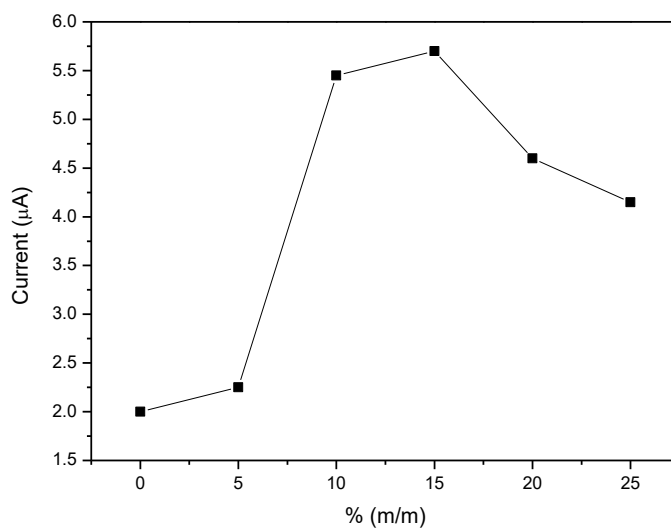


**Figure S5.** Variation of the anodic peak currents as a function of pH for detection of 1.0 × 10<sup>-4</sup> mol L<sup>-1</sup> Cu<sup>2+</sup> in MCPE/R2<sub>10%</sub>. Conditions: scan rates 10 mV s<sup>-1</sup>, pre-concentration potential -0.5 V for 300 s.

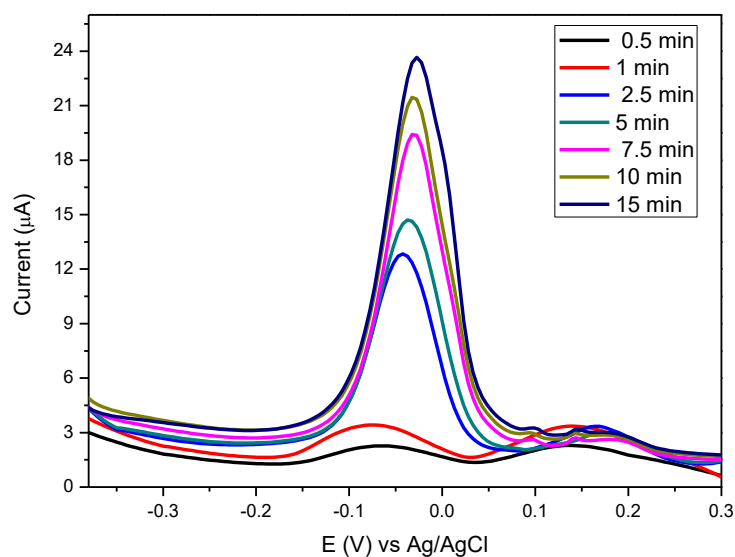


**Figure S6.** Differential pulse voltammograms of MCPE/R2<sub>10%</sub> in  $1.0 \times 10^{-4} \text{ Cu}^{2+} \text{ mol L}^{-1}$  varying of the preconcentration time. Conditions: phosphate buffer pH 6.0, scan rates  $10 \text{ mV s}^{-1}$ , pre-concentration potential  $-0.5 \text{ V}$ .

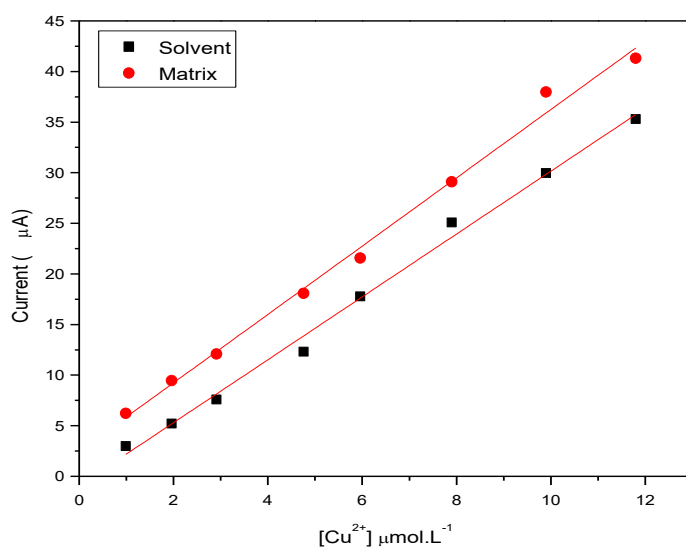


**Figure S7.** Calibration curves for electrochemical detection of  $\text{Cu}^{2+}$ , using MCPE/R2<sub>10%</sub> in the absence and presence of matrix. Conditions: phosphate buffer pH 6, scan rates  $10 \text{ mV s}^{-1}$ , pre-concentration potential  $-0.5 \text{ V}$  for 600 s.

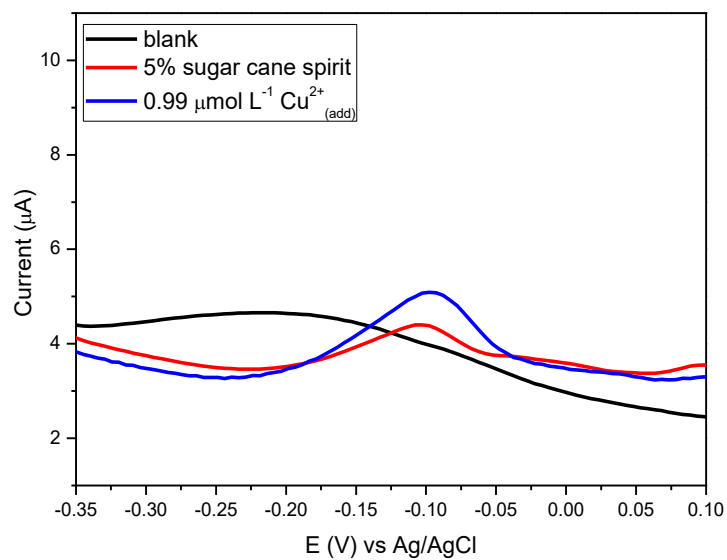


**Figure S8.** Anodic stripping differential pulse voltammograms of MCPE/R2<sub>10%</sub> in the absence of sugar cane spirit (—), 5% sugar cane spirit (—) and after addition of Cu<sup>2+</sup> (—). Conditions: phosphate buffer pH 6.0; scan rates 10 mV s<sup>-1</sup>, pre-concentration potential -0.5 V for 600 s.